Improved ODS Alloy for Heat Exchanger Tubing

Mark A. Harper
Special Metals Corporation, 3200 Riverside Drive, Huntington, WV 25705
E-mail: mharper@smcwv.com; Telephone: (304) 526-5057; Fax: (304) 526-5973

Manuscript

ABSTRACT

The Department of Energy (DOE), National Energy Technology Center (NETL), has initiated a strategic plan for the development of advanced technologies needed to design and build fossil fuel plants with very high efficiency and environmental performance. These plants, referred to as "Vision 21" by DOE, will produce electricity, chemicals, fuels, or a combination of these products, and possibly secondary products such as steam/heat for industrial use. Certain key components have been indentified as necessary for the success of a Vision 21 power plant, one of which is a high temperature heat exchanger. Thus the DOE has funded a project with the objective being to develop/produce an oxide dispersion strengthened (ODS) heat exchanger tube such that a full scale heat exchanger can be manufactured, and the alloy MA956 has been chosen for the material in this study. The major tasks related to this objective are: (a) increasing the circumferential strength of a MA956 tube, (b) joining of the MA956 tube, and (c) determining the high temperature corrosion limits of the MA956 alloy in expected Vision 21 power plant environments. This paper will discuss these topics and describe work being performed in these areas.

INTRODUCTION

Interest in increasing the efficiency of coal-fired power plants has led to the examination of alternatives to the steam boiler-Rankine cycle systems, for which increases in efficiency have been limited by both the slow progress in developing steam handling capabilities at temperatures above 565°C (1050°F) and the lack of easily-accessible sources of naturally-occurring low-temperature cooling water. Indirect-firing of gas turbines in open or closed cycles is one approach to linking the higher efficiencies possible via the Brayton cycle while still using coal as the fuel. An experimental program in the 1980's[1] demonstrated a coal-fired, low-emissions heat exchanger (fluidized-bed combustor) capable of heating air to 843°C (1550°F) in a metallic heat exchanger, and to 954°C (1750°F) or 1232°C (2250°F) with an additional ceramic heat exchanger. Current programs involving indirectly-fired gas turbine cycles are aimed at high cycle efficiencies, of the order of 47 percent based on the higher heating value (HHV) of the fuel, and involve open cycle systems in which air is heated to 760°C (1400°F) in a metallic heat exchanger, followed by further heating to 982°C (1800°F) in a natural gas-fired ceramic heat exchanger[2-4]. A variant of this approach is one where part of the coal is pyrolyzed to produce the fuel gas used to fire the ceramic heat exchanger or the turbine with air entering the turbine heated to 1288°C (2350°F). Another program envisions using a coal-fired ceramic heat exchanger for the whole duty of heating air to 1200°C (2192°F)[5].

The high temperature capabilities of the oxide dispersion strengthened (ODS) alloys would allow the size of a downstream ceramic heat exchanger to be reduced, with the possibility that more appropriate or innovative designs could be better tailored to accommodate the needs of the ceramics, especially the difficult ceramic-to-metal joints. Thus, the Department of Energy (DOE) has funded a project with the objective being the production of an ODS heat exchanger tube such that a full-scale heat exchanger can be manufactured, and the INCOLOY ® MA956 alloy has been chosen as the material for this study. The major tasks of this project are:

(a) increasing the circumferential strength of a MA956 tube,
(b) joining of the MA956 alloy, and
(c) determining the high temperature corrosion limits of the MA956 alloy in expected Vision 21 power plant environments,

which are described below.

® INCOLOY is a registered trademark of the Special Metals Corporation

Increasing the Circumferential Strength of a MA956 Tube

There have been significant developments in recent years in alloys strengthened by an oxide dispersion which can provide creep strength up to approximately 90 percent of the alloy melting temperature (T_{melt} ~ 1480°C/2696°F). The ferritic ODS alloys based on Fe-Cr-Al have the potential for application at higher temperatures than the conventionally-strengthened alloys in which the strengthening mechanisms degrade as the precipitated phases become less stable with increasing temperature. One reason for the significant increase in strength at high temperatures is due to the thermal stability and low matrix solubility of the oxide dispersion (Y_2O_3). Figure 1 shows creep rupture data for various alloys[6], including data for the MA956 alloy in the longitudinal direction. These data were calculated from 2/3 of the 10,000 hour rupture strength[7]. As shown in this figure, the strength of the MA956 alloy can be an order of magnitude greater than the best conventional wrought material at temperatures approaching 1100°C (2012°F).

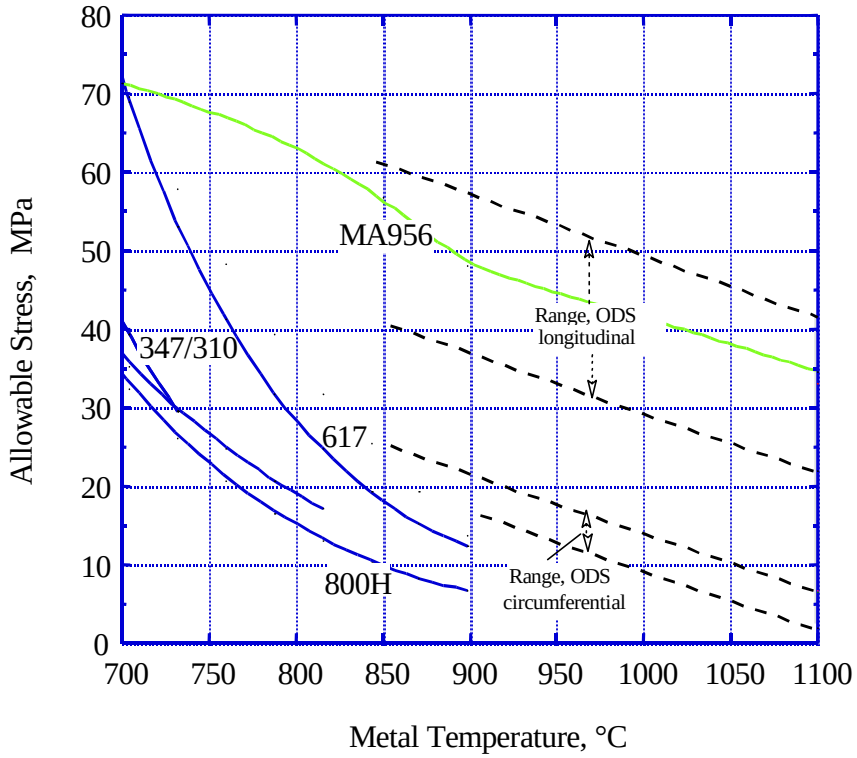

Figure 1. Allowable Stresses for Qualified and Pending ASME Boiler and Pressure Vessel Code High-Temperature Alloys (*data for MA956 and other ODS alloys were based on 2/3 10,000 hr creep rupture strength)[6].

Although the properties of the ODS alloys appear promising, available data are usually for relatively short times and none of these alloys has been BPV Code-qualified. Furthermore, as observed from Figure 1 there is a strong anisotropy in the creep strength of these alloys, with a factor of 10 difference between the longitudinal and circumferential directions[8]. This anisotropy is a result of the microstructure of these materials, in which elongated grains are produced in the longitudinal direction and a fine grain structure in the circumferential direction. The elongated grain structure results in a high percentage of the grain boundary surface area being parallel to the applied stress during testing. Plasticity theory states that plastic flow will not occur on a plane with zero resolved shear stress applied to it. A grain boundary parallel to the applied stress direction is such a plane and thus creep along such a grain boundary will not occur. In contrast, the fine grained microstructure in the circumferential direction has a high percentage of grain boundary surface area anti-parallel to the applied stress direction. Thus creep strength in this direction is poor. Progress in processing and microstructural control has resulted in increases in the circumferential creep strength, however it is still significantly lower than the strength in the longitudinal direction and the use of ODS alloys for tube applications has been restricted due to this limitation.

Joining the MA956 Alloy

The other critical limitation of the ODS alloys is the ability to satisfactorily weld these materials and produce joints that possess high temperature mechanical properties that approach the properties of the base material. The difficulties of joining ODS alloys, particularly for applications such as high temperature heat exchangers, are well recognized. Indeed, Starr *et. al*[9], noted that, "the major design constraint (for the European COST 501 Round II ODS high temperature heat exchanger) was in tube welding." The design team avoided tube-to-tube joints in the ODS material because of concerns about joint integrity, and used thick-walled stubs of cast stainless to join the ODS tubes to the cast header.

The major challenge in welding ODS alloys is to produce joints which:

- minimize agglomeration of the strengthening oxide dispersoids,
- minimize the amount of lower-strength, dispersoid-free material present at the interface, and
- maximize the amount of parent metal grain growth across the prior interface.

Melt-based techniques such as gas tungsten arc (GTA), laser and electron beam welding are generally avoided, since fusion of the ODS material produces both agglomeration of the strengthening yttria/yttrium aluminum garnet dispersoids and porosity within the molten zone. Conventional vacuum brazing uses alloys which melt at temperatures on the order of 1260°C (2300°F), and also introduces a significant amount of lower-strength phases into the joint.

Solid-state joining processes have been more successful than the melt-based techniques. Friction welding has been used to join MA965 sheet. In this process, one of the two pieces to be joined is held stationary while the other is rotated at high speed and pressed against it. The combination of frictional heating and pressure produces a solid-state joint between the two workpieces. The process is also well suited for producing tube-to-tube joints, and is used for this purpose in lower-strength steels. Additional work is needed to adapt this process for ODS tubes, however, because current practices cause the heated, softened metal to bulge outward from the joint, producing metal flow perpendicular to the longitudinal axis of the tube. The resulting transverse grain boundaries lower the creep strength of the joint.

Explosive welding has also been used successfully to join MA956 and other ODS alloys. Materials have been bonded in both the recrystallized and unrecrystallized conditions, and joint efficiencies of greater than 65% have been observed at 1100°C (2012°F)[10]. Indeed, explosive welding was used to join the ODS alloy tubes to the cast stainless stubs in the COST 501 high temperature heat exchanger. Only limited work has been done, however, to explore the use of explosive welding for tube-to-tube ODS joints and to assess the elevated temperature performance of the resulting joints. In addition, there is a need to demonstrate the ability of explosive welding to successfully join ODS tubes to the heat resistant alloy header materials required for heat exchanges designed to operate at temperatures approaching 1260°C (2300°F).

Diffusion bonding, high pressure diffusion bonding and transient liquid phase (TLP) bonding have also been used somewhat successfully to bond ODS materials. Both ferritic MA956 and austenitic MA754 sheet have been diffusion bonded into composites for defense applications[11], and high pressure diffusion bonding has been used by several investigators to join MA 956 materials[12,13]. High pressure appears to be useful, but brings with it the engineering challenges associated with avoiding macroscopic indentation of the workpiece (for applications involving hard tooling) or encapsulating the joint in a gas-tight "can" (for hot isostatic pressing).

Recent work also suggests the potential for using TLP bonding to join ferritic ODS materials for heat exchangers. Using this technique with an iron-base filler metal, Nakao and Shinozaki were able to produce butt joints in MA956 which exhibited 650°C (1202°F) tensile strengths, elongations and reductions in area comparable to those of the base alloy[14]. Similarly, Khan and Wallach have been able to produce TLP butt joints in unrecrystallized MA956 using Fe-B-Si foils or sputtered Fe-B-Si films and then used a conventional ODS recrystallization anneal to obtain parent metal grain growth across the joint interface[15]. The joints produced with the Fe-B-Si foils, however, exhibited chromium boride precipitates along the joint plane, and joints produced with both the foils and sputtered films exhibited recrystallized grain sizes smaller than those observed in unbonded materials. Elevated temperature mechanical properties of the joints were not reported.

Environmental Resistance

The ferritic ODS alloys have excellent resistance to high temperature oxidation, sulfidation, and carburization attack, but their corrosion resistance in the presence of molten alkali salts (an environment that would probably be encountered on the fire side of the heat exchanger tube) is not well established. The excellent corrosion resistance is due to the level of Al in the alloy (e.g. ~ 4.5wt%), which upon exposure to a high temperature hostile environment results in the formation of a very protective, adherent slow-growing alumina (Al_2O_3) scale. Experience with molten salt corrosion in marine gas turbines suggests that alloys which form alumina scales may exhibit lower resistance to this form of attack compared to alloys that form a chromia (Cr_2O_3) scale for protection. However, initial results from 4,000+ hour boiler probe tests suggest that some alumina scale-forming alloys (Fe_3Al) possess equivalent corrosion resistance to the best chromia-forming alloys[16]. Note, however, that this work was conducted on two Fe_3Al alloys and at relatively low temperatures (704-732°C/1300-1350°F)

Resistance of the alloys to the high-velocity working fluid also requires attention at the higher temperatures. In particular, the ability of the alloy to form a stable oxide scale that is adherent and does not produce particles of spalled oxide is critical to reducing erosion damage to the gas turbine downstream. The rate of growth of oxide scales in air is typically higher than in steam at a given metal temperature, and the composition of the scales is likely to be different as a result of the different effective oxygen partial pressures of steam and air. It is likely that the available databases for scale growth and spallation in steam will need to be supplemented (or replaced); hence, there is a need for information on scale spallation behavior in air oxidation for all of the candidate alloys. The ferritic ODS alloys have outstanding resistance to scale spallation at high temperatures[17]. Long-term oxidation testing under temperature-cycling conditions has shown that these alloys essentially do not suffer scale spallation for several thousand hours; when spallation initiates it occurs as very small particles, and the alumina scale is reformed until the aluminum in the alloy is depleted to very low levels (~ 1.5 wt%) before the onset of formation of non-protective iron-rich scales which could be a spallation-erosion threat.

A further point for consideration is that above approximately 1025°C (1877°F) in static dry air environments and at temperatures as low as 800°C (1472°F)[18] in flowing, dry air, Cr_2O_3 scale can be further oxidized to gaseous CrO_3. The rate of CrO_3 formation and subsequent loss is controlled by diffusion across the aerodynamic boundary layer[19], so that the higher the gas velocity (the thinner the boundary layer), the more rapid the loss. Furthermore, recent results[20] indicate that water vapor has a significant effect on scale volatility, such that the vapor pressure of an oxyhydroxide species, $CrO_2(OH)_2$, exceeds that of CrO_3 by many orders of magnitude at temperatures below approximately 1100°C (2012°F) in an environment containing 10 percent by volume of water vapor**.** This form of degradation not only removes chromium from the alloy, thereby affecting alloy strength as well as oxidation resistance, but also leads to deposition via condensation of CrO_3 at some point downstream, which may also be undesirable.

In high-temperature, high-gas flow applications (such as gas turbine hot gas path components), alloys or coatings that form a protective scale of the relatively non-volatile Al_2O_3 typically are used instead of Cr_2O_3-forming alloys. There are techniques that could be used to provide protective alumina scale-forming coatings on the internal surfaces of tubing, but there is limited capacity for handling long tube lengths, and any effect of the heat treatment cycle involved on alloy properties would require consideration. Since the ODS alloy MA956 is an alumina-former, it would not require a coating on the working fluid side.

EXPERIMENTAL PROCEDURE

In order to understand the effect of extrusion + thermomechanical processing parameters on the microstructure of a MA956 tube (see composition in Table 1 below), the first phase of this project will result in the completion of the matrix of tests shown in Table 2 below. After processing of these samples, the resulting microstructures are analyzed for grain size/morphology, texture, and Y_2O_3 particle distribution within the matrix. Also, creep testing is underway for the purpose of determining the "stress threshold" curves of the MA956 alloy.

Table 1
Nominal Composition (wt%) of the ODS Alloy MA956

Fe	Cr	Al	Ti	C	Y_2O_3
74	20	4.5	0.5	0.05	0.5

Table 2
Matrix of Extrusion + Cold Work + Recrystallization Parameters

Extrusion Temp (°C)	Extrusion Ratio	Amount of Cold Work (%)	Recrystallization Temp (°C)	Recrystallization Time (h)
1000	10:1	0	1000	0.5
1075	16:1	10	1150	1
1150	20:1	20	1300	6
1200		30		
		40		

Four different types of solid state joining techniques are being investigated at the present time. They are: friction welding, explosion welding, magnetic impulse welding and transient liquid phase (TLP) bonding. All of these techniques are being investigated for the ability to join the MA956 alloy to itself, and to join this material to a traditional heat resistant alloy, in particular the alloy 601.

Complementary laboratory and field exposures are being performed in environments expected to be encountered by the external and internal surfaces of MA956 tubes in service. With respect to the working-fluid side of the tube wall (i.e. the I.D.), laboratory exposures in air are being conducted in order to measure kinetic data and determine the criteria (such as aluminum consumption, change in oxidation rate, and initiation of scale spallation) that would signify the end of service life as governed by oxidation resistance. Regarding fireside corrosion of the MA956 alloy, both laboratory and actual field testing will be conducted in order to study the effects of various synthetic flue gases and deposits that are expected to be encountered in Vision 21 plants. In laboratory exposures, data will be obtained and analyzed in order to determine the kinetics, failure criteria for the MA956 alloy, and to develop a wastage prediction model for the material in each gas and deposit environment. The field exposures will use air-cooled exposure probes in an actual-coal fired combustion system to generate 10,000-hour data on the corrosion resistance to the fireside environment. Also, the air-cooled probes will expose the MA956 tube samples to prototypical boiler conditions with atmospheric air on the working fluid side.

RESULTS AND DISCUSSION

Creep Strength

Referring to Table 2 in the previous section and the matrix of tests to be performed, Table 3 shows the work completed to date. At shown in this table, relatively few of the final microstructures have been analyzed. However, analysis thus far does show trends between processing parameters and the final microstructure do exist. For example, regarding the effect of recrystallization temperature, samples annealed at 1000°C did not exhibit any recrystallization, independent of the amount of cold work imposed on the sample. However, samples annealed at 1150°C did show the onset of primary recrystallization with the amount being dependent on the amount cold work. When annealed at 1300°C, all the samples exhibited primary and secondary recrystallization, with the final recrystallized grain morphology being a function of the cold work for a given sample. Figure 2 shows the variation in microstructure morphology observed as a function of cold work for samples annealed 1300°C for six (6) hours. Although sufficient data is not yet available to allow for an understanding and quantitative prediction of the effect of the various production variables on the final component microstructure, this knowledge will be critical in producing a tube with the desired microstructure and thus desired mechanical properties.

Results of the creep testing of specimens cut in the axial direction from the walls of a nominal 1 inch diameter MA956 tube are shown in Figure 3. As shown on this Larsen-Miller plot, the data being generated in this program is in agreement with data in the literature. The next step in this task has been to generate data from the transverse direction of the tube by taking a 2.5'' OD x 0.25'' wall thickness tube, cutting it in half and then flattening the two halves such that samples can be take in the transverse direction. Figure 4 shows a plot of the creep data generated thus far from these samples and compared to the data generated in the longitudinal direction. As shown in this graph, the transverse properties are inferior to the longitudinal properties as expected.

Table 3
Work Completed on Extrusion Campaign

Operation	Number Required	Number Complete	% Complete
Extrusion	180	180	100
Decanning	540	540	100
Cold Work	540	540	100
Annealing	540	500	92
Microstructure Analysis	540		

(a)

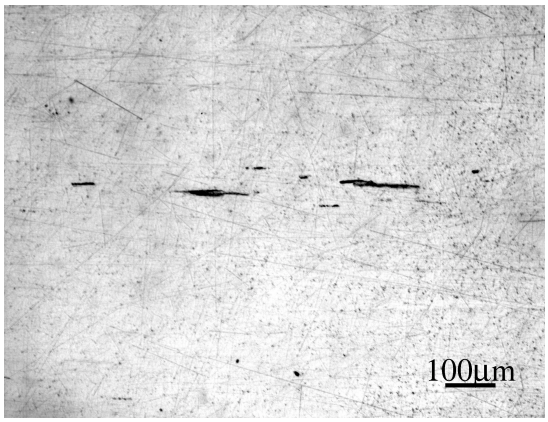

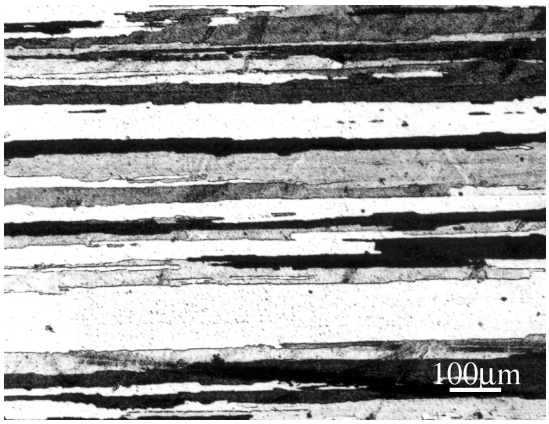

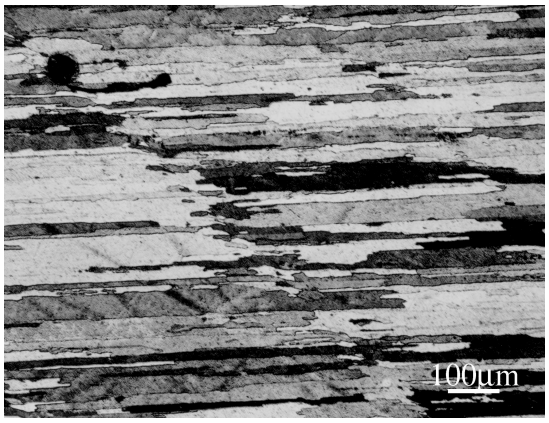

(b) (c)

Figure 2. Variation in microstructure for MA956 rods extruded at 1000°C using a 20:1 extrusion ratio followed by (a) 0% CW, (b) 10% CW, and (c) 30% CW, and then annealed at 1300°C for 6 hours.

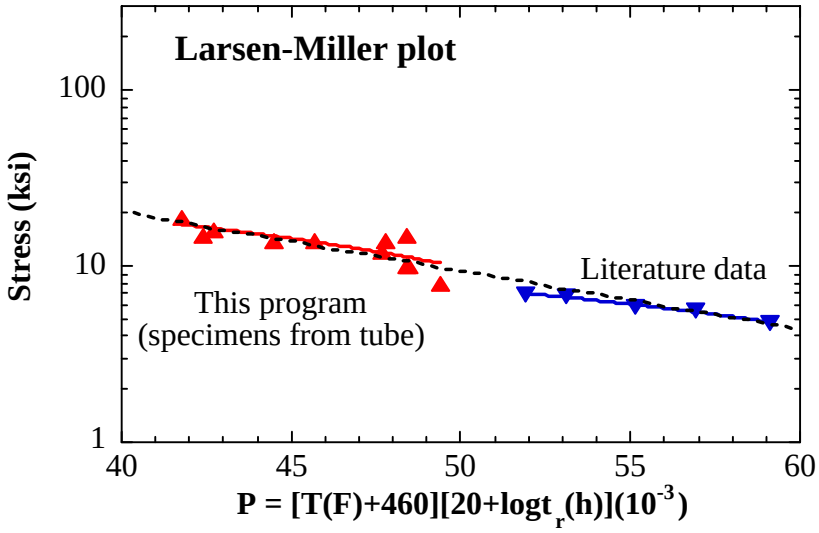

Figure 3. Larsen-Miller plot showing the good agreement between the stress rupture data obtained from this program and stress rupture data obtained from the literature.

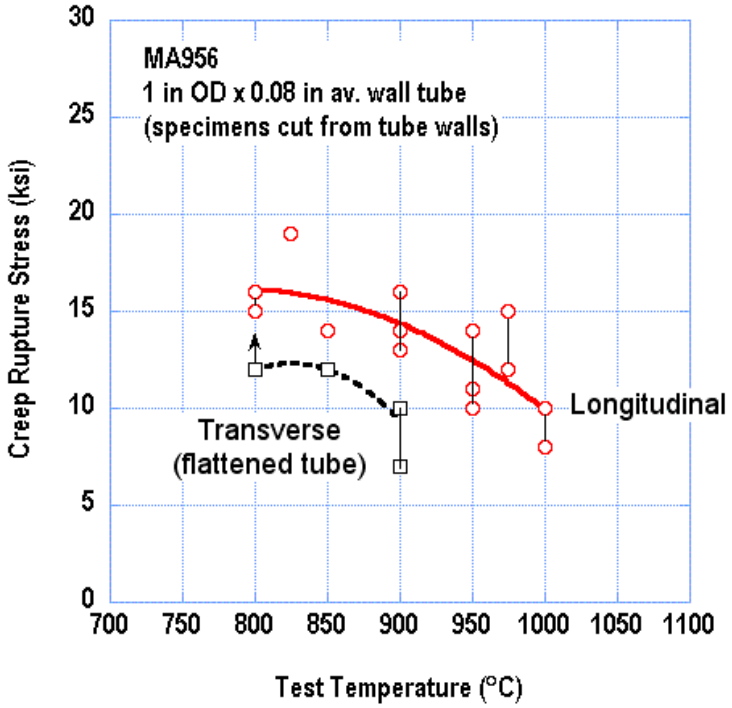

Figure 4. Comparison of longitudinal versus transverse creep rupture data for alloy MA956 tubing.

Joining the MA956 Alloy

Friction Welding: A series of welds were made on commercially available MA956 tubing and metallographic analysis and tensile tests were conducted on samples welded with two different sets of welding parameters (noted as #I2 and #I3). For tensile testing, a strip sample was taken from various points around the diameter of the tube (noted as A, B, and C). Mechanical property data for each of the welds tested are listed in Table 4. These results appear promising compared to the parent alloy properties shown in the table, however work is underway to determine cause of the variation in mechanical properties around the circumference of the joint.

Table 4
Mechanical Property Data for Two Inertia Welds

Sample Identification	Ultimate Tensile Strength (ksi)	Yield Strength (ksi)	Elongation (%)
I2-A	99.0	85.8	4.4
I2-B	73.3	N/A	0.2
I2-C	97.1	93.3	2.2
I3-A	80.0	N/A	3.4
I3-B	99.4	80.1	7.7
I3-C	67.0	N/A	2.0
MA956*	93.5	80.2	10

* Typical properties of parent material

Explosive Welding: Two samples from MA956 plate explosion welded to MA956 plate, and two samples from MA956 plate joined to 601 plate were extracted for metallographic analysis and shear testing. Figure 5 shows the interface of the MA956/MA956 and MA956/601 welds after a post explosion weld heat treatment at 1000°C for 1 hour. As shown in these micrographs, the wave-shaped interface characteristic of a successful explosion weld is present. Table 5 shows the results of the shear testing performed on the as-welded samples and the post weld heat-treated samples. The heat-treated MA956/MA956 sample showed a slight decrease in bond strength as a result of the heat treatment whereas the MA956/601 sample showed an increase in shear bond strength after the heat treatment. However, the measured shear strength for the heat treated MA956/601 sample may be artificially high due to the relatively high ductility of the annealed 601 material. The next step will consist of weld trials on the tube materials of the MA956 and 601 alloys using nearly identical explosion welding parameters as for the plate samples.

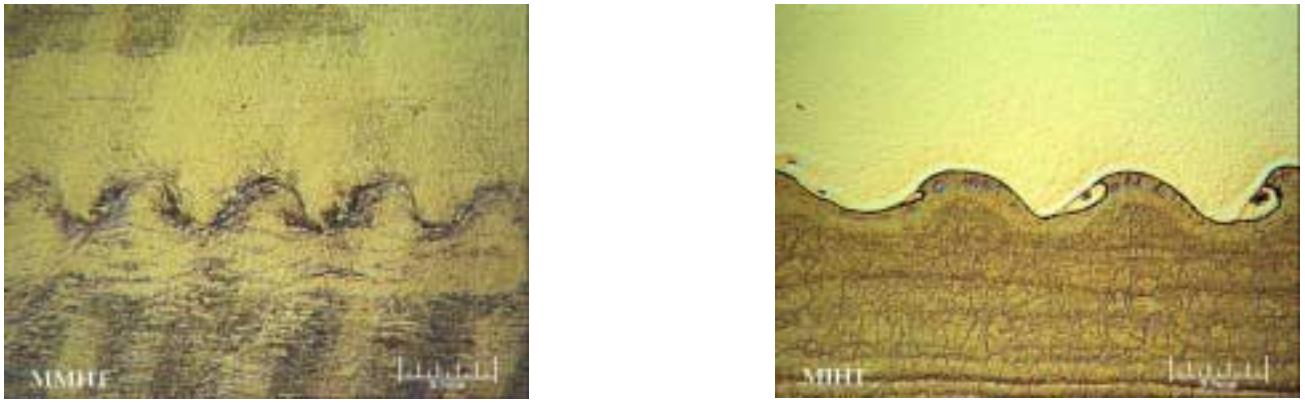

(a) MA956/MA956 (b) MA956/601

Figure 5. Optical micrographs of the interface of an explosion weld between (a) MA956 and MA956 plate and (b) MA956 and 601 plate.

Table 5
Shear Test Results of Explosion Welds Made on MA956 plate to MA956 plate and MA956 Plate to 601 Plate

Sample	Shear Strength (ksi)
MA956/MA956	82.0
MA956/MA956 + Heat Treatment*	77.2
MA956/601	79.5
MA956/601 + Heat Treatment*	88.7**

* Heat treatment performed at 1000°C for 1 hour

** Value may be artificially high due to ductility of the 601 after the 1000°C/1 hour heat treatment

Magnetic Impulse Welding: Joining trials using ½ inch diameter rod has shown this process to be feasible to join the MA956 alloy, however higher impact velocities may be needed and thus a new concentrator is being built for this purpose.

Transient Liquid Phase Bonding: Work continued on the MA956 diffusion bonding trials using the vacuum hot press. This included three additional test runs on the press itself, six exploratory bonding trials on 0.5 inch diameter bar, and initiation of an eight-run parametric study designed to identify the most important process variables in diffusion bonding of the MA 956 alloy. The six exploratory bonding trials included joining borided recrystallized rod to unrecrystallized rod, borided unrecrystallized rod to recrystallized rod, and recrystallized rod to unrecrystallized rod using a thin interlayer of elemental boron. Several of these samples show significantly stronger evidence of grain growth across the prior joint interface. Figure 6 shows the bond line of the fifth bonding trial. The parametric study was designed to obtain preliminary information on the relative importance of several major diffusion bonding parameters, including final recrystallization temperature, bonding hold time at 1200°C, surface finish, and bonding pressure. The bonded samples will be evaluated by measuring the linear fraction of grains growing across the joint interface and Figure 7 shows the bond line of the second (112001-2) and fifth (112001-5) samples. These two samples have widely varying processing parameters. Sample 112001-2 is a borided/nonborided pair prepared with an 800-grit finish and recrystallized at 1340°C, whereas sample 112001-5 is boron-free, prepared with a 1200-grit finish and recrystallized at 1260°C. Not surprisingly, the two samples show significantly different behavior. Sample 112001-2 has what appears to be boriding remnants along the bond line, yet exhibits a fully recrystallized structure on both sides of the joint with some grain growth across the bond line. Sample 112001-5 exhibits a somewhat cleaner interface (presumably because it has no boride remnants), but does not appear to be fully recrystallized and shows little or no grain growth across the bond interface.

Environmental Resistance

Laboratory Testing for Working Fluid Side: Exposures of the MA956 alloy to air at very high temperatures are being conducted in order to develop a lifetime prediction model for this material. Testing at 1300°C has been completed and five samples (out of a total of seven) of different thickness taken from MA956 bar stock and exposed at 1250°C in air have failed with testing at 1200 and 1100°C currently being performed also. The observed oxidation-limited lifetimes at 1300 and 1250°C are shown in Figure 8, with data points for a similar set of samples of the MA956HT alloy included for comparison. Note that the data points with arrows indicate runs that are still in progress, and that the oxidation lifetime will be longer than presently indicated by those points. The lifetimes of MA956 and MA956HT alloys at 1250°C appear to be more than double those at 1300°C. The coincidence of the 1250°C lifetimes for MA956 with the 1300°C data points for MA956HT indicate that the latter alloy has a 50°C advantage at these very high temperatures.

Data such as those shown in Figure 8 are being used in the development of the lifetime prediction model as shown in Figure 9. The lifetime calculations were based on a two-stage oxidation model developed using data for the alloy MA956HT (Fe-21.5Cr-5.8Al-0.5Y_2O_3), but using the oxidation rates (parabolic and linear stages) and transition oxide thickness measured for the MA956 alloy. The model appears to fit well with the data, except for the thinnest specimen. The only difference from the fit used for MA956HT alloy was a change in the factor that qualifies the rate exponent in the 'linear' oxidation phase (f_{n3}) from 0.06 to 0.03. Obviously, the oxidation lifetime of MA956 at 1300°C in air is significantly lower than that of MA956HT in this testing. The important difference between the two alloys appears to be that the rate of oxidation (in Stage 2 and Stage 3) is higher for the MA956 alloy. Since both alloys form the same oxide, the reason for this difference is not obvious. The oxidation rate of

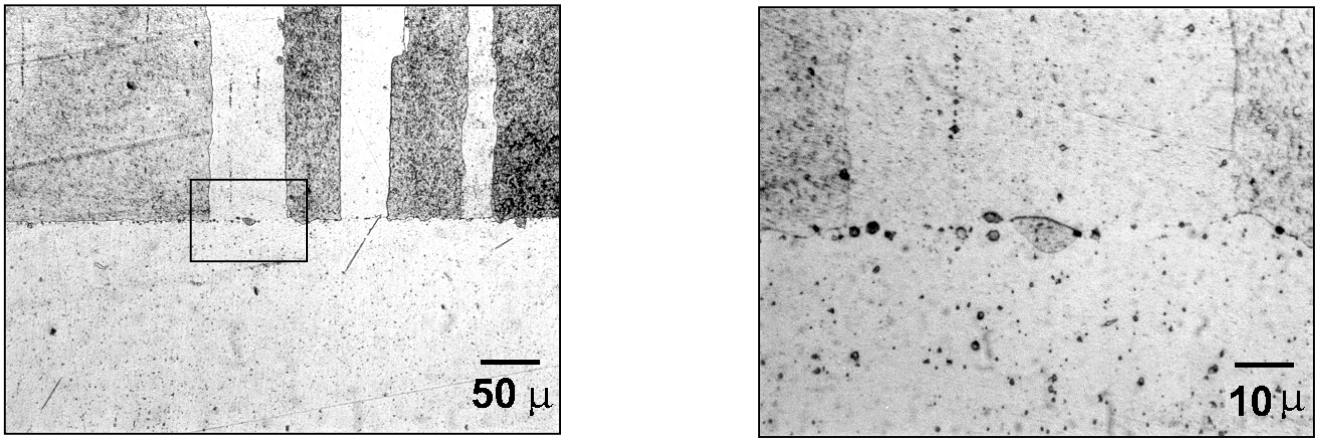

(a) (b)

Figure 6. (a) Micrograph of borided, recrystallized MA956 (top) bonded to non-borided, non-recrystallized MA956. Box in (a) shows approximate region shown in (b). Samples etched with HCl.

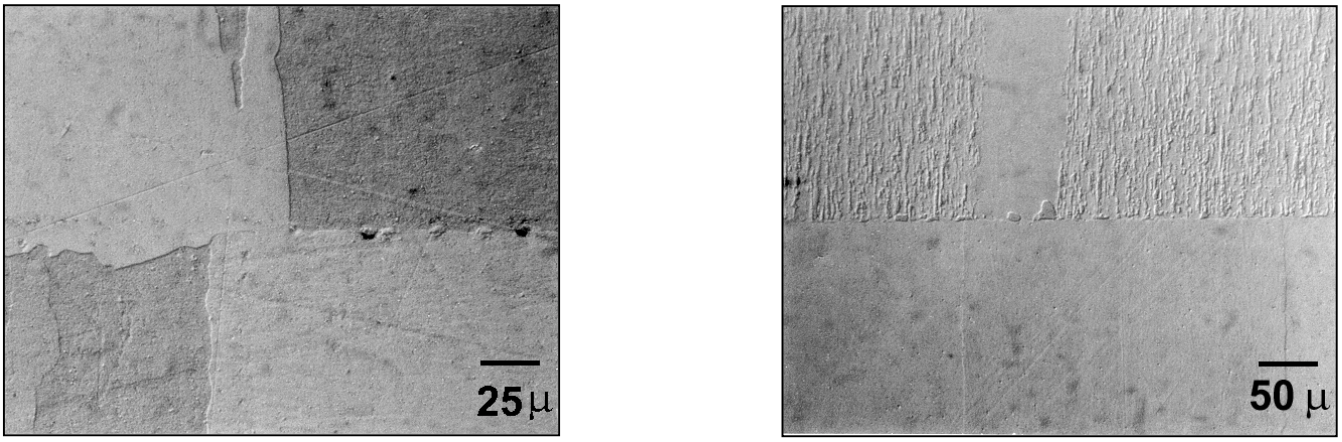

(a) (b)

Figure 7. Micrograph of (a) borided, recrystallized MA956 (bottom) bonded to non-borided, non-recrystallized MA956, and (b) non-borided, recrystallized MA956 (bottom) bonded to non-borided, non-recrystallized MA956. Samples prepared using vibratory polish and etched with HCl.

alumina-forming alloys can be significantly affected by doping with reactive elements such as Y, but the Y levels for the MA956 and MA956HT samples used in this testing are essentially the same (0.40 and 0.38 weight percent, respectively). Specimens will be prepared for examination of the structure and compositions of the alloy-oxide interface and the oxide grain boundaries by TEM.

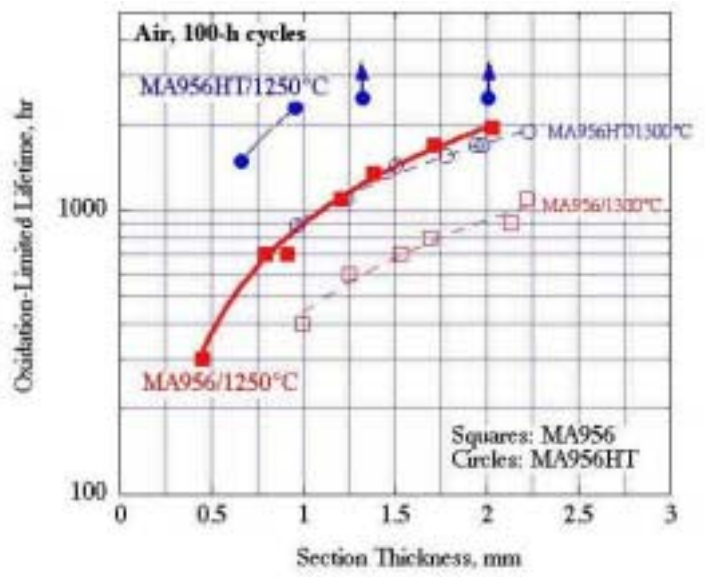

Figure 8. Plot of oxidation lifetimes as a function of sample thickness for the MA956 and MA956HT alloys at 1250°C and 1300°C in air.

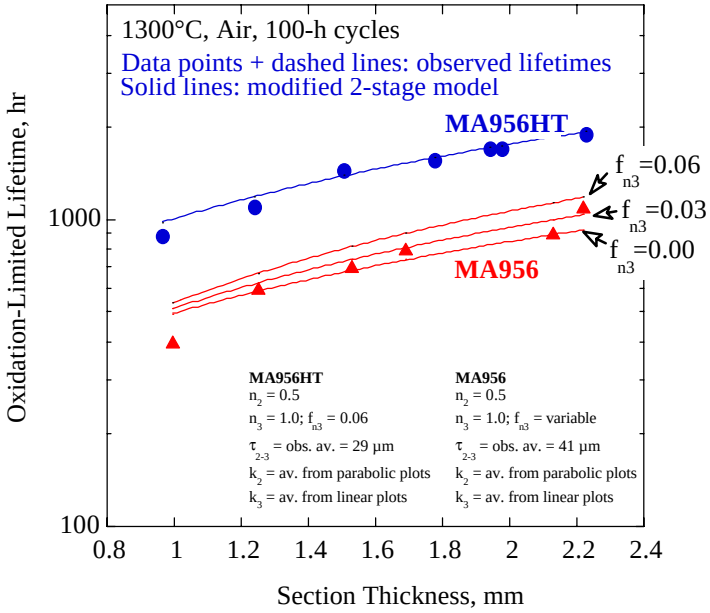

Figure 9. Comparison of oxidation lifetimes of MA956 and MA956HT at 1300°C in air as a function of specimen thickness. The data points indicate observed lifetimes. The solid line is the fit of a two-stage model developed based on data for MA956HT.

Laboratory Testing for Fireside Environment: The laboratory testing using two different flue gases and three different deposits (see Table 6 and 7 below) at 2000°F continues. The exposure of the samples is terminated every 100 hours for deposit replenishment and at 500 hours one set of samples was removed for metallurgical examination. To date the test has completed 600 hours of the 1000-hour exposure and metallurgical examination of the 500-hour samples has been initiated

Table 6
Flue Gas Compositions to be Used in Laboratory Fireside Testing

Species	Amount (vol %)	
	Gas Mixture 1	Gas Mixture 2
O_2	4	2
CO_2	15	15
H_2O	10	5
SO_2	0.25	1.0
N_2	Bal	Bal

Table 7
Deposit Compositions to be Used in Laboratory Fireside Testing

Species	Amount (wt%)		
	Ash 1	Ash 2	Ash 3
SiO_2	14.6	11.6	7.6
Al_2O_3	6.0	6.0	6.0
TiO_2	0.3	0.3	0.3
Fe Oxide	1.3	1.3	1.3
CaO	3.3	3.3	3.3
MgO	0.3	0.3	0.3
Na_2O	0.4	1.4	2.4
K Oxide	0.3	1.3	2.3
SO_3	1.2	2.2	3.2
P_2O_5	0.3	0.3	0.3
KCl			1.0
Carbon	72.1	72.1	72.1

Field Exposure Testing: The first utility with the appropriate locations for the air-cooled probes have been determined, the control hardware procured, and the probe design finalized and assembly initiated.

SUMMARY AND CONCLUSIONS

No technical conclusions are available at this time, however the change in grain morphology as a function of the extrusion + TMP parameters for the MA956 extrusions look promising with respect to developing a quantitative understanding of their effect on the final microstructure. Also, the friction welding, explosive welding, and TLP bonding are showing promising results thus far. The oxidation studies at 1300°C are complete and further high temperature corrosion tests are being conducted.

ACKNOWLEDGEMENTS

This paper was prepared ith the support of the U.S. Department of Energy, under Award No. DE-FC26-00NT40970. However, opinions, findings, conclusions, or recommendations expressed herein are those of the author and do not necessarily reflect the views of the DOE. The author also wishes to acknowledge the other team members of this program, whose work is reported in this paper: Larry Brown from the Edison Welding Institute, Jefferey Blough from the Foster Wheeler Development Corporation, Bimal Kad from the University of California at San Diego, Marvin McKimpson from the Michigan Technological University, and Ian Wright from the Oak Ridge National Laboratory.

REFERENCES

1. Campbell, J., Jr., and Lee, J. C., "Fired Heater Versus CCGT/Cogeneration Cycle Parameters," ASME Paper No. 82-GT-187 (1982).
2. Klara, J. M., "HIPPS: beyond state-of-the-art, Part I," *Power Engineering*, 12, 37-39 (1993).
3. Klara, J. M., "HIPPS can compete with conventional PC systems: Part II," *Power Engineering*, 13, 20-23 Jan (1994).
4. Robson, F. L., Ruby, J., and Seery, D. J., "Repowering with High-Performance Power Plant Systems (HIPPS)," pp. 162-167 in *Proc. Pittsburgh Coal Conf.*, Sep. 1996.
5. LaHaye, P. G., Strom-Olsen, J., Seger, J. L., and Pickup, H., "Externally-Fired Combined Cycle Demonstration", in *Proc. Advanced Coal-Fired Power Systems '95 Review Meeting*, H.M. McDaniel, D.J. Mollot, and V.K. Venkataraman, Eds., DOE/METC-95/1018, pp. 55-64, June 1995 (1995).
6. Wright, I. G. and Stringer, J., "Materials Issues for High-Temperature Components in Indirectly-Fired Cycles", ASME Paper No. 97-GT-300 (1997)
7. McColvin, G. M., and Smith, G. D., "Environmental Resistance of Incoloy Alloy MA956," pp. 139-153 in *High-Temperature Alloys*, J. B. Marriott et al., Eds., Elsevier, New York (1987).
8. Private communication to I.G. Wright from R. C. Hurst, Joint Research Centre, Petten, The Netherlands (1996).
9. Starr, F., White, A. R., and Kazimierzak, B., "Pressurized Heat Echangers for 1100^{o}C Operation Using ODS Alloys", (in) D. Coutsouradis, et. al. (eds.) *Materials for Advanced Power Engineering 1994*, Boston, Kluwer Academic Publishers, p. 1393 (1994).
10. deBarbadillo, J. J., and Smith, G. D., "Recent Developments and Challenges in the Application of Mechanically Alloyed, Oxide Dispersion Strengthened Alloys", (in) P. Shingu, (ed.) *Mechanical Alloying*, Brookfield VT, Trans Tech Publications, p. 167 (1992).
11. Testin, R. A., Ewing, B. A., and Speers, J. A., "A High-Performance Austenitic ODS Alloy Sheet for Gas Turbine Applications", (in) *Superalloys 1992*, Warrendale, PA, The Metallurgical Society, p. 83 (1992).
12. Bucklow, I. A., "Diffusion Bonding of a Creep-Resisting Ferrous ODS Alloy", *Advances in Joining Newer Structural Materials*, Elmsford, NY, Pergamon Press, p. 299 (1990).
13. Stover, D., *et. al*, "HIP Diffusion Bonding of ODS Materials", (in) R. J. Schaefer and M. Linzer, (eds.) Hot Isostatic Pressing: Theory and Applications, Metals Park, OH, ASM International, p. 217 (1991).
14. Nakao, Y., and Shinozaki, K., "Transient Liquid Phase Diffusion Bonding of Iron Base Oxide Dispersion Strengthened Alloy MA956", *Materials Science and Technology*, Vol. 11, p. 304 (1995).
15. Khan, T. I., and Wallach, E. R., "Transient Liquid Phase Diffusion Bonding and Associated Recrystallization Phenomena When Joining ODS Ferritic Superalloys", *J. Material Science*, Vol. 31, p. 2937 (1996).
16. Blough, J. L., and Stanko, G.J., "Fireside Corrosion Testing of Candidate Superalloy Tube Alloys, Coatings, and Claddings – Phase II", Presented at the *Tenth Annual Conf. On Fossil Energy Materials*, Knoxville, TN, May 1996 (1996).
17. Quadakkers, W. J., Bongartz, K., Schubert, F., and Schuster, H., pp. 1533-1542 in *Materials for Advanced Power Engineering 1994*, D. Coutsouradis, et al., Eds., Kluwer Academic Publishers (1994).
18. Lowell, C. E., "A Scanning Electron Microscope Study of the Surface Morphology of TD-NiCr at 800°C to 1200°C," *Oxid. of Met.*, 5 (3), 205-219 (1972).
19. Graham, H. C., and Davis, H. H., *J. Am. Ceram. Soc.*, 54, 89 (1971).
20. Opila, E. J., and Jacobson, N. S., "Volatile Hydroxide Species of Common Protective Oxides and Their Role in High-Temperature Corrosion," Presented at the *ECS Symp. on Fundamental Aspects of Corrosion VI*, San Antonio, Texas, Oct. 1996 (1996).